Weissel, J., Peirce, J., Taylor, E., Alt, J., et al., 1991
Proceedings of the Ocean Drilling Program, Scientific Results, Vol. 121

25. ANALYSIS OF THE AUSTRALASIAN MICROTEKTITE EVENT, THE TOBA LAKE EVENT, AND THE CRETACEOUS/PALEOGENE BOUNDARY, EASTERN INDIAN OCEAN[1]

J. Smit,[2] A.J.M. van Eijden,[2] and S. R. Troelstra[2]

ABSTRACT

The Toba lake event, the Australasian microtektite event, and the Cretaceous/Paleogene boundary were analyzed on the basis of foraminifers, carbonate content, trace elements, and spherules (microtektites). The Toba ash event, recovered in Hole 758C, may have had minor influences on the foraminiferal populations. The Australasian tektite event has probably some influence on foraminiferal ecology, because the larger specimens become scarce just above the microtektite layer. Microtektites recovered from Hole 758B closely resemble spherules recovered from several Cretaceous/Paleogene boundary localities in North America. The Cretaceous/Paleogene spherules, however, are usually larger and are completely altered to goyazite in the terrestrial environment and to smectite in a marine environment.

The Cretaceous/Paleogene boundary of Hole 752B does not show obvious anomalous trace-element concentrations, and iridium concentrations are below our detection limits. The trace-element pattern is dominated by the alternation of chalk with volcanic ash layers above the Cretaceous/Paleogene boundary.

INTRODUCTION

The authors investigated several sample sets across important geological events recovered during Ocean Drilling Program Leg 121. The Toba lake volcanic eruption event (75,000 yr ago) was sampled about every 3 cm in Hole 758C. The Australasian tektite event (0.7 m.y. ago) was sampled every 4 cm in Hole 758B. The Cretaceous/Paleogene (K/Pg) boundary was sampled in Holes 758A and 752B. A large hiatus of about 2 m.y. at the K/Pg boundary of Hole 758A prevented a detailed study. The high volcanic ash content in the K/Pg interval in Core 121-752B-11R resulted in complete destruction of planktonic foraminifers, and no new results were obtained besides those reported in Peirce, Weissel, et al. (1989). The Quaternary events were sampled to gain better insight in the catastrophic event at the K/Pg boundary and its biological consequences.

TOBA LAKE EVENT

Samples of 1 cm^3 were taken every 3 cm across the ash layer in Hole 758C in Section 121-758C-1H-2, which is visible in the core at 1.33–1.85 m below seafloor (mbsf). This ash layer is believed to be the ash layer from the Toba lake eruption which took place 75,000 years ago. The Toba lake eruption is one of the largest eruptions both in magnitude and amount of erupted magma in the Quaternary. The amount of erupted magma is estimated at 2000 km^3 dense rock equivalent (Ninkovich et al., 1979; Dehn, this volume). This amount is about 20 times more than the ash produced by the eruption of Tambora in 1813, the largest in historic times. Tambora has led to some climate changes in the years following the eruption. We investigated whether the Toba lake eruption produced observable changes in the planktonic foraminiferal populations. Some feldspar and other minerals of the Toba eruption are supposedly shock-metamorphosed (Carter et al., 1986), and this is taken as an indication that shock-metamorphosed minerals from the K/Pg boundary may be derived from cataclysmic volcanic eruptions, instead of a large impact event.

We analyzed the washed residues of the samples above and below the Toba tephra layer and determined the $CaCO_3$ content. The carbonate content did not change significantly across the Toba ash layer (Table 1, Fig. 1). Although all faunas are partly dissolved, quantitative counts (Table 2) of the (least affected) >250 mm fraction show some interesting, but not easily interpretable patterns. The important foraminiferal changes are plotted in Figure 1 along with the $\delta^{18}O$ curve of SPECMAP (Imbrie et al., 1984), which reflects ice volume changes in this interval. Most of the observed changes in the sampled interval are probably related to these ice volume changes. The probable effects of the Toba lake event on the foraminiferal populations are difficult to separate from those of the onset of the last glaciation, which begins slightly after the Toba eruption.

The deeper dwelling *Globorotalia menardii* and *G. tumida* are more dissolution resistant than the thinner-walled *Globigerinoides ruber, G. trilobus,* and *G. sacculifer.* The latter group is significantly more abundant above the Toba ash layer, and this is not easily explained by ice volume changes alone. *Pulleniatina obliquiloculata* is the dominant foraminifer in almost all samples, especially above the Toba ash. This species is also thick-walled and probably relatively dissolution resistant. Yet this species shows a pattern comparable with the *G. ruber* group, rather than the *G. menardii* group. A dissolution index may be interpreted from the abundance of whole tests vs. broken tests of planktonic foraminifers (Fig. 1). Planktonic tests are also more easily dissolved than benthic foraminiferal tests, and fluctuations in the P/B ratio follow the fragmentation index of planktonic tests. This index shows a rather sudden jump across the Toba ash, and may indicate that the lysocline became shallower as a consequence of the Toba eruption.

AUSTRALASIAN MICROTEKTITE EVENT

A set of 32 samples of 1 cm^3 each was analyzed from Sections 121-758B-2H-1 and 121-758B-2H-2 (9.95–11.36 mbsf) for Australasian microtektites, carbonate, and planktonic foraminifers. The results are shown in Tables 3 and 4. Glass (1969, 1982) showed that microtektites from the Australasian tektite strewn field occur close to the Brunhes/Matuyama magnetic reversal. This reversal was determined aboard ship in Hole 758B at 10.65 mbsf. The purpose of this study was to find out whether or not the

[1] Weissel, J., Peirce, J., Taylor, E., Alt, J., et al., 1991. *Proc. ODP, Sci. Results,* 121: College Station, TX (Ocean Drilling Program).

[2] Geomarine Center, Instituut voor Aardwetenschappen, de Boelelaan 1085, 1081 HV Amsterdam, Netherlands.

Table 1. $CaCO_3$ analyses across Toba ash in Hole 758C.

Core, section, interval (cm)	Depth (mbsf)	$CaCO_3$ (%)
121-758C-		
1H-1, 123	1.23	53.90
1H-1, 126	1.26	55.90
1H-1, 125	1.29	45.90
1H-1, 132	1.32	52.40
1H-1, 135	1.35	49.50
1H-1, 138	1.38	45.20
1H-1, 141	1.41	48.80
1H-1, 144	1.44	45.30
1H-1, 147	1.47	46.40
1H-2, 1	1.51	37.80
1H-2, 3	1.53	25.80
1H-2, 6	1.56	12.70
1H-2, 9	1.59	0.10
1H-2, 18	1.68	1.50
1H-2, 31	1.81	2.50
1H-2, 32	1.82	62.10
1H-2, 36	1.86	61.60
1H-2, 39	1.89	60.90
1H-2, 42	1.92	61.30
1H-2, 45	1.95	63.50
1H-2, 48	1.98	62.40
1H-2, 51	2.01	61.60
1H-2, 54	2.04	57.20
1H-2, 57	2.07	59.40
1H-2, 60	2.10	64.90
1H-2, 63	2.13	57.50
1H-2, 66	2.16	57.70
1H-2, 69	2.19	58.70
1H-2, 72	2.22	59.30
1H-2, 75	2.25	70.20
1H-2, 78	2.28	65.90
1H-2, 81	2.31	67.20
1H-2, 84	2.34	65.40
1H-2, 87	2.37	64.00
1H-2, 90	2.40	62.00
1H-2, 99	2.49	57.20
1H-2, 109	2.59	60.60
1H-2, 119	2.69	58.30
1H-2, 129	2.79	58.50
1H-2, 139	2.89	58.60
1H-2, 149	2.99	60.10

major and recent impact event that produced the Australasian tektites had any influence on the ecology of planktonic foraminifers. Analysis of the microtektites could give a better insight in the microtektite-like spherules found worldwide at the K/Pg boundary. Carbonate content was measured by dissolving 200 mg of each sample in 10N HCl, and measuring the resulting CO_2 pressure. Results are checked with pure $CaCO_3$ standards and blanks. Reproducibility is within 1%. More than 1000 microtektite samples were recovered and some of these were analyzed on an electron microprobe, and a JEOL-SEM equipped with a Link 6400 X-ray dispersive analyzer (Table 5). Quantitative counts of planktonic foraminifers were considered unreliable, due to strong dissolution signatures, rather strong bioturbation, and the scarcity of mature specimens in the >250 mm fraction. The microtektites are scattered across a 63-cm interval from 10.45 to 11.08 mbsf, with the peak concentration centered at 10.95 mbsf (Fig. 2). According to the analysis of Officer and Lynch (1983), the original depth of deposition of the microtektite layer should be about 11 cm above the lowest occurrence of microtektites, at about 10.97 mbsf. This is about 32 cm below the Brunhes/Matuyama boundary at 10.65 mbsf in Hole 758B. The upper part of the microtektite peak is abnormally truncated by the volcanic ash layer at 10.75–10.65 mbsf. The yield of microtektites from the samples in that interval is lower due to dilution by the ash.

The >40-mm fraction was further subdivided in three fractions: 40–125 mm, 125–250 mm, and >250 mm (Fig. 3 and Table 4). The profiles of these residue fractions are disturbed by the two ash layers at 11.3 and 10.8 mbsf.

The percentage of the >250-mm grain-size fraction is dominated by planktonic foraminifers. Only a few pumice fragments occur in the >250-mm fraction. At about 10.85 mbsf the abundance of larger, mature specimens decreases. This decrease probably coincides with the microtektite peak, just below the upper ash layer. The drop in abundance of large, mature specimens of foraminifers suggests a relation with the Australasian event. Qualitatively, however, there is no relation between planktonic foraminifers and the Australasian event. Further analysis of stable oxygen and carbon isotopes of individual foraminifers in this sample set is in progress.

The microtektites display a variety of forms (Pl. 1). Most microtektites are spherical (84%); 4% are flat ellipsoids, 3% strongly elongate, 9% droplets (Fig. 4), and a few have a dumbbell (Pl. 1, Fig. 1) or highly irregular shape. Twenty-four percent of the microtektites are broken specimens, especially the larger ones (Fig. 5) and the droplets (Table 3 and Fig. 2). All microtektites are transparent and are entirely glassy. No internal relict or newly formed quench crystals have been observed. The color varies from dark brown to crystal clear. The mean size of the spheroidal microtektites is about 0.15 mm. The largest microtektites are invariably broken. The maximum size of these broken microtektites is about 0.6 mm (Fig. 5). Some microtektites contain bubble cavities (Pl. 1, Fig. 6). The microprobe results are given in Table 5. These agree well with the major element composition of Australasian microtektites from other areas (Cassidy et al., 1969). The lower totals of our analysis in comparison with microprobe analysis of Cassidy et al. (1969) is striking. Some volatile constituent (water?) is probably present in the microtektites of Hole 758B, which is surprising, regarding the common opinion that tektites consist of virtually volatile-free glass.

About 7% of the microtektites show flowlines on the surface (Fig. 4). These flowlines are visible because the surface of most of the microtektites is etched. (Pl. 1, Figs. 5–6; Pl. 2, Figs. 1–2). Apparently slight differences in composition of the tektite glass leads to differential dissolution on the surface (Glass, 1974). The microtektites apparently are broken before deposition in the sediment because the flowlines are also etched out on the fractures (Pl. 1, Figs. 3–4; Pl. 2, Fig. 1). Stress developed during cooling in flight of the microtektites may have been responsible for most of the fracturing.

The flow structures and bubble cavities in the Australasian microtektites provide important links with spherules from the K/Pg boundary in North America. These K/Pg spherules are problematic, considered by some (Smit, 1984; Bohor et al., 1987) to be altered microtektites and by some (Izett, 1987) to be purely authigenic. Smit (1984) found kaolinitic spherules in the kaolinitic K/Pg boundary claystone bed of the Hell Creek area in Montana and in the Raton Basin, Colorado, and considered these to be altered microtektites. Bohor et al. (1987) described abundant spherules in a similar K/Pg boundary claystone layer at Dogie Creek, Wyoming. The Wyoming spherules have a form similar to the spherules at Hell Creek and Raton Basin, but are larger and are much more abundant (Izett, 1987). These spherules are now altered and consist of a hollow goyazite shell, which is void or filled with various secondary minerals, such as gypsum (Fig. 6). At Dogie Creek the K/Pg boundary claystone can be traced in the field over several hundred meters. The kaolinitic claystone bed with spherules contains anomalous amounts of iridium (1.6 ng/g) and is directly overlain by the "magic" impact layer, a similar, thinner claystone that contains even more iridium (>20.8 ng/g), and shocked minerals (Bohor et al., 1987). This dualistic nature

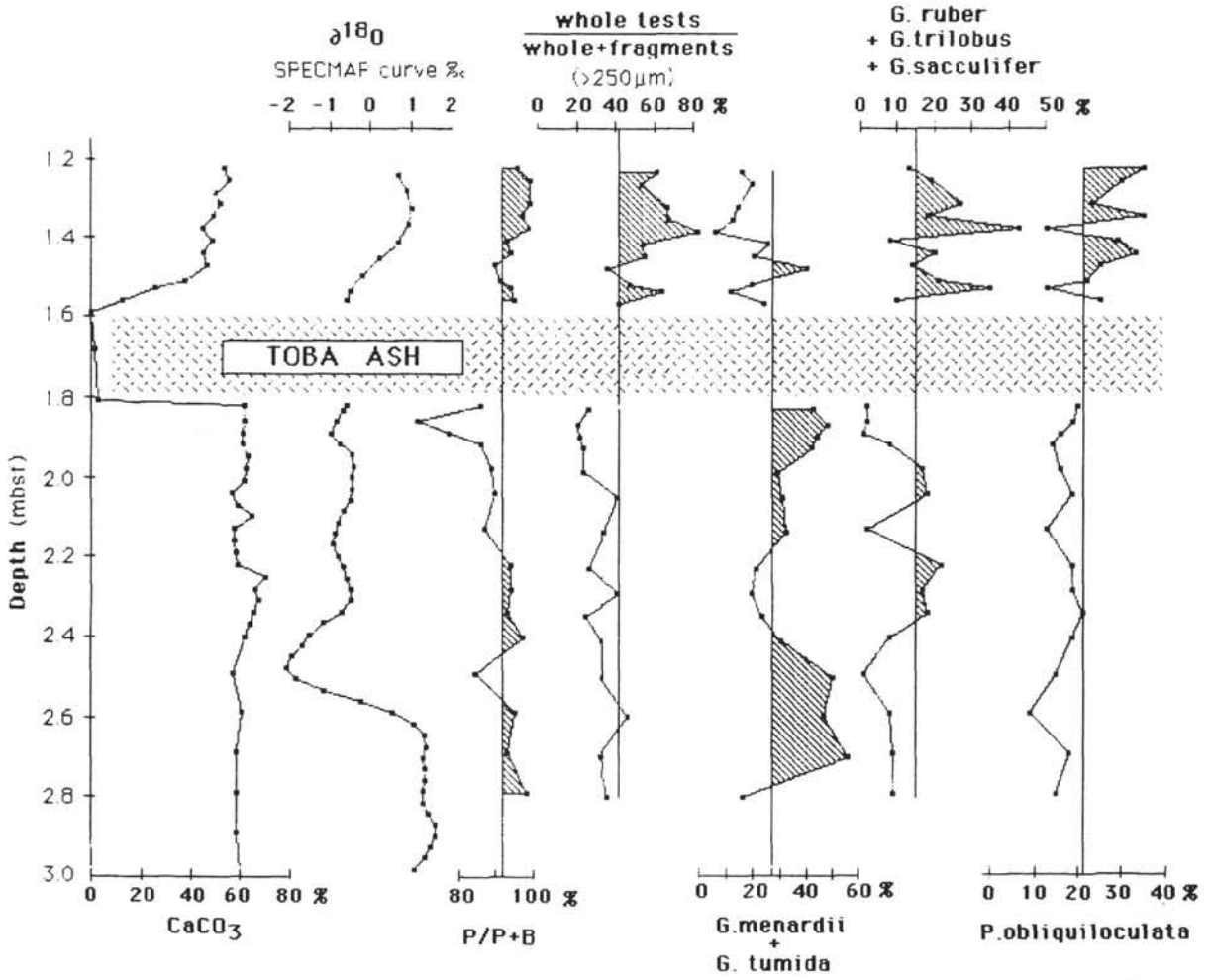

Figure 1. $CaCO_3$ profile, relative abundances of the most important foraminiferal groups (data from Table 1), the number of dissolved tests (wh/wh + frag x 100), and the ratio of planktonic vs. benthic foraminifers (P/P + B x 100) across the Toba ash layer of Hole 758C. The $\delta^{18}O$ SPECMAP curve (Imbrie et al, 1984) is calibrated against a sedimentation rate of 21 mm/k.y. (ash to surface) above, and 14 mm/k.y. (ash to Brunhes/Matuyama reversal) below the ash layer. Values above the mean are shaded.

of the K/Pg boundary claystone is a typical characteristic of the K/Pg boundary in continental facies all over North America (Izett, 1987). We have also collected thousands of these spherules in Dogie Creek and studied these in washed residue and thin sections. The most common forms are spherical (>90%), and most are close to 1 mm in size (Fig. 6). The goyazite usually has grown from the original outer wall toward the interior of the spherule (Fig. 6A), probably by replacement of the original material. Infilling of a cavity left in the claystone after dissolution of the original spherule is considered less likely, as subsequently shown. Former "cracks" within a spherule are commonly lined by goyazite. Goyazite also grows from the wall of cavities that occur frequently within the spherules (Fig. 6B–C). Here the goyazite grows outward from the wall of the cavity. The majority of these cavities are perfectly spherical and smooth and shiny on the inside. Most cavities are still empty, but some are filled by secondary minerals (barite) or filled with a second generation of goyazite. The spherical cavities within the goyazite spherules are analogous to the bubble cavities commonly observed in the Australasian microtektites (Pl. 2, Fig. 5).

About 5% of the Dogie Creek spherules are droplet-shaped (Pl. 2, Figs. 5–6). Many of the spherules and droplets show flowlines on the surface, which resemble the flowlines found on the surface of Australasian microtektite droplets. Spherules and droplets of the same size as the goyazite spherules at Dogie Creek were found at the K/Pg boundary of Site 603 (Klaver et al, 1987). These spherules are not altered to goyazite, which is typical for a continental weathering of tropical soils (Izett, 1987), but are altered to a ferruginous smectite. The construction of these smectite spherules is almost identical as the goyazite spherules, and presume a similar alteration sequence of the glass precursor. In these smectite spherules the original internal bubble cavities are preserved.

Von der Borch (1970) reported numerous basaltic microlapilli from Miocene-Oligocene deposits in Site 31, close to an oceanic spreading center. These microlapilli also display spherical and droplet shapes, and are of the same size as the K/Pg goyazite spherules. The Site 31 microlapilli are associated with numerous angular volcanic shards and irregular pumice fragments of the same composition. They are microcrystalline and do not show flowlines on the surface. Although there are some resemblances, it is less likely that the K/Pg spherules could be explained as microlapilli. Moreover, the K/Pg spherules are transported subaerially, are far from a basaltic source, and are spread out over a much larger area that the Site 31 microlapilli. In summary, the goyazite and smectite spherules from the K/Pg boundary and the

Table 2. Foraminiferal abundances in Hole 758C.

Depth (mbsf)	*P. obliquiloculata*	*G. menardii*	*G. tumide*	*G. dutertrei*	*G. ruber*	*G. trilobus*	*G. sacculifer*	*G. conglomerata*	*S. dehiscens*	*H. aequilateralis*	*G. conglobatus*	Planktonic	Benthic	Number	P/B ratio
1.23	35	14	2	16	7	4	2	12	1	4	2	3	4	198	96
1.26	30	17	2	8	10	8	1	14	3	2	4	2	1	195	99
1.32	23	11	3	12	9	17	1	15	3	2	1	3	1	184	99
1.35	35	10	2	15	6	12	0	10	3	2	2	2	3	184	97
1.38	13	5	0	26	19	21	3	9	0	2	1	1	1	209	99
1.41	29	14	11	9	1	5	2	16	4	2	8	1	7	196	94
1.44	33	15	5	10	8	9	4	12	1	2	2	1	6	198	95
1.47	25	12	27	8	6	7	1	5	1	1	4	1	10	146	91
1.51	22	11	8	18	12	7	2	8	1	2	5	3	9	147	92
1.53	13	8	3	24	18	15	2	4	0	1	0	11	6	97	94
1.56	25	13	11	23	6	4	0	6	2	2	2	6	5	127	95
1.82	20	18	25	9	1	1	1	15	5	2	1	3	14	130	88
1.86	19	15	33	4	0	2	0	15	4	1	6	1	31	125	76
1.89	16	18	26	10	0	1	0	20	3	2	3	1	23	143	81
1.92	14	26	16	13	3	5	0	17	4	2	1	2	14	132	87
1.98	16	18	11	15	4	11	2	15	1	1	5	1	11	141	90
2.04	19	23	9	6	6	12	0	13	4	2	5	3	10	124	91
2.13	13	24	8	18	1	1	0	29	1	1	2	2	13	91	88
2.22	19	16	4	24	8	12	2	8	2	1	3	1	6	185	94
2.28	19	10	9	21	5	12	0	12	1	4	2	6	6	174	95
2.34	21	20	4	18	12	7	0	11	1	3	2	3	7	196	94
2.40	19	22	7	15	2	3	2	20	1	3	3	2	3	178	97
2.49	15	28	22	1	0	1	0	21	3	2	5	3	16	148	87
2.59	9	26	22	13	4	4	0	13	4	1	1	3	5	167	95
2.69	18	25	31	6	2	7	0	6	1	1	2	1	7	153	93
2.79	15	13	3	43	1	8	0	8	2	4	0	2	2	242	98
Mean	21	17	12	15	6	8	1	13	2	2	3	2	9	162	92

Australasian microtektites have many features in common. Therefore, it seems likely that both are formed in the same way, as impact products.

CRETACEOUS/PALEOGENE BOUNDARY

The K/Pg boundary was possibly completely recovered in Section 121-752B-11R-3, 94 cm, at 385.75 mbsf. Although no obvious hiatus exists, an unknown amount of sediment may be missing at the frequent drilling biscuits (Rea et al., 1990). The K/Pg sequence in Hole 752B seems complete, based on the biostratigraphy of the calcareous nannofossils and the magnetostratigraphy (Gee et al., chapter 16, this volume). The replacement of Cretaceous species by "disaster" species and new Paleogene species is identical to what is observed in other complete K/Pg sequences (Pospichal, this volume). A complete K/Pg boundary in the Southern Ocean was previously recovered at Leg 113 Site 689 and Hole 690C at Maud Rise (Barker, Kennett, et al., 1988) and at Site 750 on the Kerguelen Plateau (Schlich, Wise, et al., 1989). At all these sites a considerable iridium anomaly was measured (Michel et al., this volume).

Trace elements of 13 samples across the K/Pg boundary were analyzed by instrumental neutron activation analysis (INAA). The analytical methods are described in Smit and ten Kate (1982) (Figs. 7–9). We have looked further (in vain) for microtektites and other spherules (Smit and Romein, 1985), and we tried to obtain useful washed residues by various standard methods from the K/Pg interval. The Upper Cretaceous samples were fairly easy to disaggregate, but none of the samples from the dark, ash-rich interval from Samples 121-752B-10R-6, 25 cm, to 121-752B-11R-3, 94 cm (352.9–358.75 mbsf), yielded any prepared clean residues. Foraminifers in thin section were crushed beyond recognition.

The results of the INAA analyses are presented in Table 6. The distribution of the analyzed (trace) elements is dominated by the volcanic ash (Figs. 7–9). The iridium content in all of the samples is below the detection limit of the INAA analysis (about 10 ng/g). Most elements follow the distribution of carbonate and volcanic ash, and elements apparently associated with the ash (Fig. 7) (Na, K, Co, Fe, Cr, Sr, and Ba) show parallel trends with the volume magnetic susceptibility measurements (Peirce, Weissel, et al., 1989), which supposedly reflect the concentration of magnetic volcanic minerals. As, Sb, Co, Cr, and Ni (Fig. 8) are elements that usually show enhanced values at the K/Pg boundary (Smit and ten Kate, 1982). Only As shows a slightly higher value precisely at the K/Pg boundary in Hole 752B, but the amounts are still small compared with other K/Pg boundary sites. The REE all show the same pattern, somewhat comparable with the distribution of Sc, Hf, Ta, and Th (Fig. 9). The association with volcanic material of these elements is not clear. The highest values are not coincident with the maximum ash concentration. La/Yb is high in the chalks and low in ash layers. This suggests that most of the REE in the ash-rich samples is indeed derived from the ash itself. In the chalk most of the REE is from other sources. Presumably most is precipitated from ocean water by adsorption on falling particles.

CONCLUSIONS

1. Some changes in the abundances of planktonic foraminifers may be due to the Toba lake eruption, which was probably the most severe volcanic eruption in the Quaternary. No species disappear from the area and the changes observed are not easily separated from those effects caused by the onset of the last major glaciation.

2. The Australasian tektite event similarly may have had some influence on the abundance of larger, mature planktonic foraminifers. No foraminiferal species disappear, but the decrease of larger specimens suggests some deleterious effect on the biosphere as a result of this minor impact event.

Table 3. Carbonate and microtektite abundances in Hole 758B.

Core, section, interval (cm)	Depth (mbsf)	$CaCO_3$ (%)	Sample weight (g)	A	B	C	D	E	F	G
121-758B-										
2H-1, 45	9.95	58.90	1.06	0	0	0	0	0	0	0
2H-1, 55	10.05	47.20	0.81	0	0	0	0	0	0	0
2H-1, 71	10.21	55.80	1.14	0	0	0	0	0	0	0
2H-1, 75	10.25	53.10	0.99	0	0	0	0	0	0	0
2H-1, 79	10.29	58.00	0.84	0	0	0	0	0	0	0
2H-1, 83	10.33	57.80	0.96	0	0	0	0	0	0	0
2H-1, 86	10.36	56.40	0.69	0	0	0	0	0	0	0
2H-1, 90	10.40	56.30	0.45	0	0	0	0	0	0	0
2H-1, 95	10.45	54.50	0.90	1	1	0	0	0	0	1
2H-1, 99	10.49	55.00	0.94	1	1	0	0	0	0	0
2H-1, 103	10.53	49.70	1.11	4	2	0	1	1	0	0
2H-1, 107	10.57	54.70	1.06	2	2	0	0	0	0	0
2H-1, 111	10.61	47.70	0.85	0	0	0	0	0	0	0
2H-1, 115	10.65	41.00	0.72	1	0	0	0	0	1	0
2H-1, 119	10.69	26.80	0.75	0	0	0	0	0	0	0
2H-1, 125	10.75	0.00	1.06	0	0	0	0	0	0	0
2H-1, 135	10.85	1.20	1.57	73	45	2	3	9	14	0
2H-1, 137	10.87	55.70	0.59	104	67	1	2	1	32	4
2H-1, 141	10.91	55.90	0.81	199	114	3	2	12	62	0
2H-1, 145	10.95	56.60	0.58	145	85	5	2	13	34	2
2H-1,148	10.98	52.60	0.43	179	121	4	3	10	38	1
2H-2, 1	11.00	53.70	0.59	86	60	5	3	6	10	0
2H-2, 4	11.04	53.20	0.74	132	77	4	2	12	35	3
2H-2, 8	11.08	50.90	0.89	40	24	2	1	2	11	4
2H-2, 12	11.12	52.90	0.78	0	0	0	0	0	0	0
2H-2, 16	11.16	56.20	0.84	0	0	0	0	0	0	0
2H-2, 20	11.20	50.60	0.87	0	0	0	0	0	0	0
2H-2, 24	11.24	1.90	0.77	0	0	0	0	0	0	0
2H-2, 28	11.28	19.60	0.89	0	0	0	0	0	0	0
2H-2, 32	11.32	50.00	0.65	0	0	0	0	0	0	0
2H-2, 36	11.36	55.60	1.07	0	0	0	0	0	0	0
Totals				963	600	26	19	66	237	15

Note: A = total recovered microtektites > 125 μm; B = spheres; C = ellipsoids; D = strongly elongate; E = droplets; F = number of broken microtektites; G = number of microtektites > 250 μm.

3. The similarity in form (spheroids, droplet-shape, flowlines, and bubble cavities) between the Australasian microtektites and goyazite/smectite spherules from the K/Pg boundary in North America suggest a corresponding origin. The K/Pg goyazite/smectite spherules were originally probably made of glass and subsequently altered into different minerals.

4. Neutron activation data of the K/Pg boundary show little enhancement of elements (Ni, Co, Cr, As) which are known to be enriched elsewhere at the K/Pg boundary.

ACKNOWLEDGMENTS

The authors wish to thank T. van Meerten for the INAA analyses, M. Konert, P. H. Willekes, R. van Elzas for laboratory analyses, S. Kars for help on the SEM, W. Lustenhouwer for microprobe analyses, and T. van Kempen for preparation of the goyazite and smectite spherules. Reviews by F. T. Kyte and B. P. Glass are greatly appreciated.

REFERENCES

Barker, P. F., Kennett, J. P., et al., 1988. *Proc. ODP, Init. Repts.*, 113: College Station, TX (Ocean Drilling Program).

Bohor, B. F., Triplehorn, D. M., Nichols, D. J., and Milard, H. T., Jr., 1987. Dinosaurs, spherules, and the "magic" layer: a new K-T boundary clay site in Wyoming. *Geology*, 15:896–899.

Carter, N. L., Officer, C. B., Chesner, C. A., and Rose, W. I., 1986. Dynamic deformation of volcanic ejecta from the Toba caldera: possible relevance to the Cretaceous-Tertiary boundary phenomena. *Geology*, 14:380–383.

Glass, B. P., 1982. Possible correlation between tektite events and climatic changes? *Spec. Pap. Geol. Soc. Am.*, 190:251–258.

Imbrie, J., Hays, J. D., Martinson, D. G., McIntyre, A., Mix, A. C., Morley, J. J., Pisias, N. G., Prell, W. L., and Shackleton, N. J., 1984. The orbital theory of Pleistocene climate: support from a revised chronology of the marine delta $\delta^{18}O$ record. In Berger, A., Imbrie, J., Hays, J., Kukla, G., and Saltzman, B. (Eds.), Milankovitch and Climate (Pt. 1): Dordrecht (D. Reidel), 269–305.

Izett, G. A., 1988. The Cretaceous-Tertiary (K-T) boundary interval, Raton Basin, Colorado and New Mexico, and its content of shock-metamorphosed minerals: implications concerning the K-T boundary impact-extinction theory. *Open-File Rep. U.S. Geol. Surv.*, No. 87-606.

Klaver, G. T., van Kempen, T.M.G., Bianchi, F. R., and van der Gaast, S., 1986. Green spherules as indicators of the Cretaceous/Tertiary boundary in Deep Sea Drilling Project Hole 603B. *In* van Hinte, J. E., Wise, S. W, Jr., et al., *Init. Repts. DSDP*, Washington (U.S. Govt. Printing Office), 93:1039–1056.

Ninkovich, D., Sparks, R.S.J., and Ledbetter, M. T., 1979. The exceptional magnitude and intensity of the Toba eruption, Sumatra: an example of the use of deep-sea tephra layers as a geological tool. *Bull. Volcanol.*, 41:286–297.

Officer, C. B., and Lynch, D. R., 1983. Determination of mixing parameters from tracer distributions in deep-sea cores. *Mar. Geol.*, 52:59–74.

Peirce, J., Weissel, J., et al., 1989. *Proc. ODP, Init. Repts.*, 121: College Station, TX (Ocean Drilling Program).

Rea, D. K., Dehn, J., Driscoll, N., Farrell, J., Janecek, T., Owen, R. M., Pospichal, J. L., Resiwati, P., and the ODP Leg 121 Scientific Party, 1990. Paleoceanography of the eastern Indian Ocean from ODP Leg 121 drilling on Broken Ridge. *Geol. Soc. Am. Bull.*, 102:679–690.

Schlich, R., Wise, S. W., Jr., et al., 1989. *Proc. ODP, Init. Repts.*, 120: College Station, TX (Ocean Drilling Program).

Smit, J., 1984. Evidence for worldwide microtektite strewnfield at the Cretaceous Tertiary boundary. *Geol. Soc. Am. Abst. Prog.*, 16:650. (Abstract)

Smit, J., and Romein, A.J.T., 1985. A sequence of events across the Cretaceous-Tertiary boundary. *Earth Planet. Sci. Lett.*, 74:155–170.

Smit, J., and ten Kate, W.G.H.Z., 1982. Trace element patterns at the Cretaceous-Tertiary boundary—consequences of a large impact. *Cretaceous Res.*, 3:307–332.

von der Borch, C. C., 1970. Glassy objects in deep sea clays. *In* McManus, D. A., Burns, R. E., et al., *Init. Repts. DSDP*, Washington (U.S. Govt. Printing Office) 5:525–531.

Date of initial receipt: 27 February 1990
Date of acceptance: 1 August 1990
Ms 121B-149

Table 4. Carbonate and washed residue weight percentages in Hole 758B.

Core, section, interval (cm)	Depth (mbsf)	$CaCO_3$ (%)	Residue (%)	>250 μm (%)	125–250 μm (%)	<125 μm (%)
121-758B-						
2H-1, 45	9.95	58.9	20.8	17.6	18.9	48.9
2H-1, 55	10.05	47.2	28.2	12.2	11.3	67.0
2H-1, 71	10.21	55.8	16.7	24.9	17.5	45.5
2H-1, 75	10.25	53.1	15.5	15.0	21.6	49.7
2H-1, 79	10.29	58.0	20.5	15.0	22.0	49.7
2H-1, 83	10.33	57.8	19.6	20.3	18.2	42.2
2H-1, 86	10.40	56.3	18.0	6.3	13.8	51.3
2H-1, 90	10.36	56.4	28.2	17.4	23.1	51.8
2H-1, 95	10.45	54.5	19.3	16.2	20.8	54.3
2H-1, 99	10.49	55.0	12.9	9.8	14.8	50.0
2H-1, 103	10.53	49.7	18.1	13.5	18.5	54.5
2H-1, 107	10.57	54.3	32.5	16.8	22.0	56.2
2H-1, 111	10.61	47.7	18.4	7.7	13.5	59.0
2H-1, 115	10.65	41.0	25.4	10.4	14.3	61.5
2H-1, 119	10.69	26.8	32.6	5.3	9.4	71.3
2H-1, 123	10.73	14.0	33.3	3.7	8.6	71.7
2H-1, 125	10.75	0.0	61.9	0.4	0.9	89.8
2H-1, 135	10.85	1.2	69.1	11.2	5.0	38.2
2H-1, 137	10.87	55.7	32.9	26.9	23.3	38.9
2H-1, 141	10.91	55.9	26.1	28.8	20.8	40.1
2H-1, 145	10.95	56.6	32.2	30.5	21.9	39.0
2H-1, 148	10.98	52.6	26.1	26.1	15.3	36.9
2H-2, 1	11.00	53.7	30.8	25.8	20.9	41.2
2H-2, 4	11.04	53.2	18.3	24.4	14.8	39.3
2H-2, 8	11.08	50.9	15.4	19.0	16.1	46.7
2H-2, 12	11.12	52.9	15.2	21.2	4.0	50.8
2H-2, 16	11.16	56.2	20.0	30.5	18.0	43.7
2H-2, 20	11.20	50.6	22.2	33.2	17.6	42.5
2H-2, 24	11.24	1.9	52.9	7.1	35.1	53.6
2H-2, 28	11.28	19.6	44.1	5.9	41.9	47.8
2H-2, 32	11.32	50.0	21.7	9.9	25.5	53.2
2H-2, 36	11.36	55.6	15.4	8.5	11.0	53.0
Average		45.4	27.0	16.3	17.5	51.2

Table 5. Microprobe analyses of Australasian microtektites.

Sample	A center	A edge	A edge	B center	B edge	B edge	C center	C edge	C edge	D center	D edge	D edge	E center	E edge	F center	Australasian microtektites (Cassidy et al., 1969) Range Maximum	Minimum
SiO_2	65.10	64.90	64.70	66.90	69.40	67.80	64.10	65.00	59.40	64.70	66.00	59.10	61.40	61.60	61.60	75.9	60.5
Al_2O_3	15.40	15.70	15.80	13.40	12.20	12.80	16.50	16.60	19.20	15.90	15.30	16.60	15.70	15.50	15.70	21.7	7.5
FeO	5.66	5.50	5.49	5.46	4.48	4.93	5.45	5.35	6.63	5.50	5.11	5.87	5.46	5.46	6.27	8.1	3
MgO	2.85	2.83	2.91	3.27	2.73	3.04	3.20	2.99	4.05	2.35	2.02	9.37	8.54	8.59	3.00	7	2.2
CaO	2.68	2.65	2.54	2.37	2.07	2.20	1.91	1.82	2.23	2.69	2.54	2.65	2.53	2.53	1.94	5.8	1
Na_2O	0.94	1.10	1.25	1.15	0.95	1.04	1.20	0.95	1.18	1.01	0.98	0.47	0.44	0.47	1.01	2.8	0.4
K_2O	2.81	2.83	2.77	2.45	2.55	2.52	2.75	2.86	2.30	2.99	3.04	0.60	0.58	0.60	3.96	3.5	0.4
TiO_2	0.73	0.85	0.81	0.71	0.60	0.64	0.75	0.77	0.98	0.79	0.85	0.96	0.85	0.83	0.73	1	0.5
MnO	0.04	0.07	0.04	0.07	0.04	0.07	0.07	0.07	0.14	0.07	0.05	0.07	0.08	0.11	0.07	0.1	0.1
BaO	0.07	0.05	0.07	0.03	0.05	0.06	0.09	0.03	0.07	0.08	0.05	0.05	0.05	0.03	0.05		
Total	96.28	96.48	96.38	95.81	95.07	95.10	96.02	96.44	96.18	96.08	95.94	95.74	95.63	95.72	94.33	102.4	97.1

Note: A–F = different individual microtektites, all from Sample 121-758B-2H-1, 141 cm.

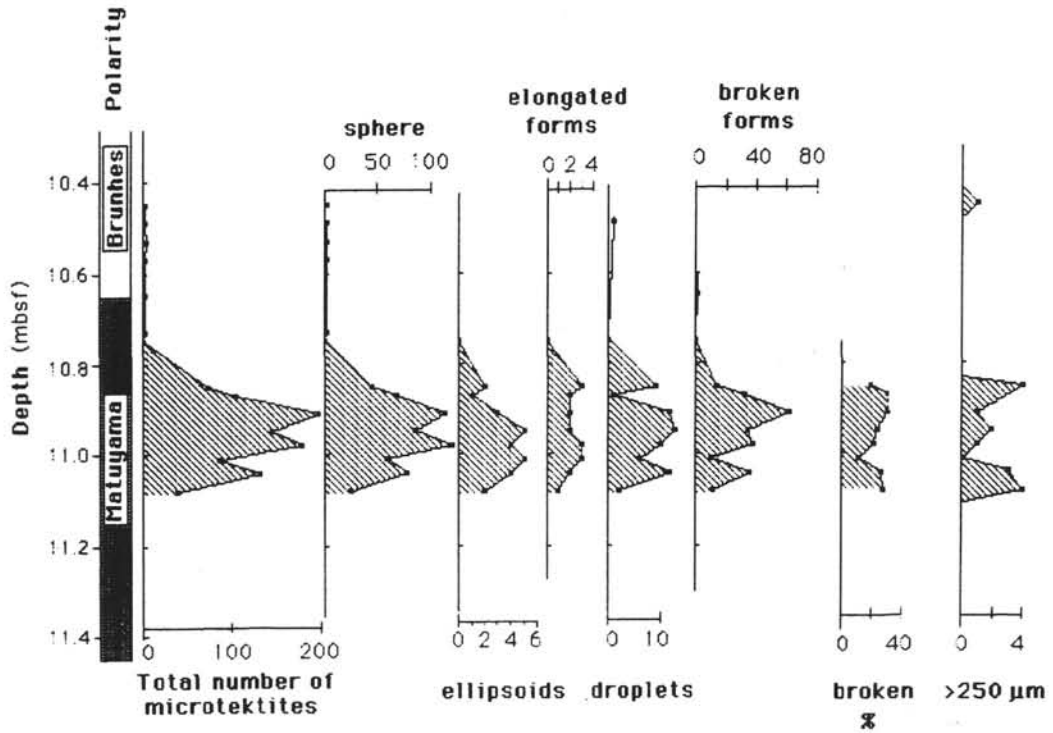

Figure 2. Number of microtektites recovered from Sections 121-758B-2H-1 and 121-758B-2H-2. The total number of microtektites in each sample is plotted because all samples have approximately the same weight.

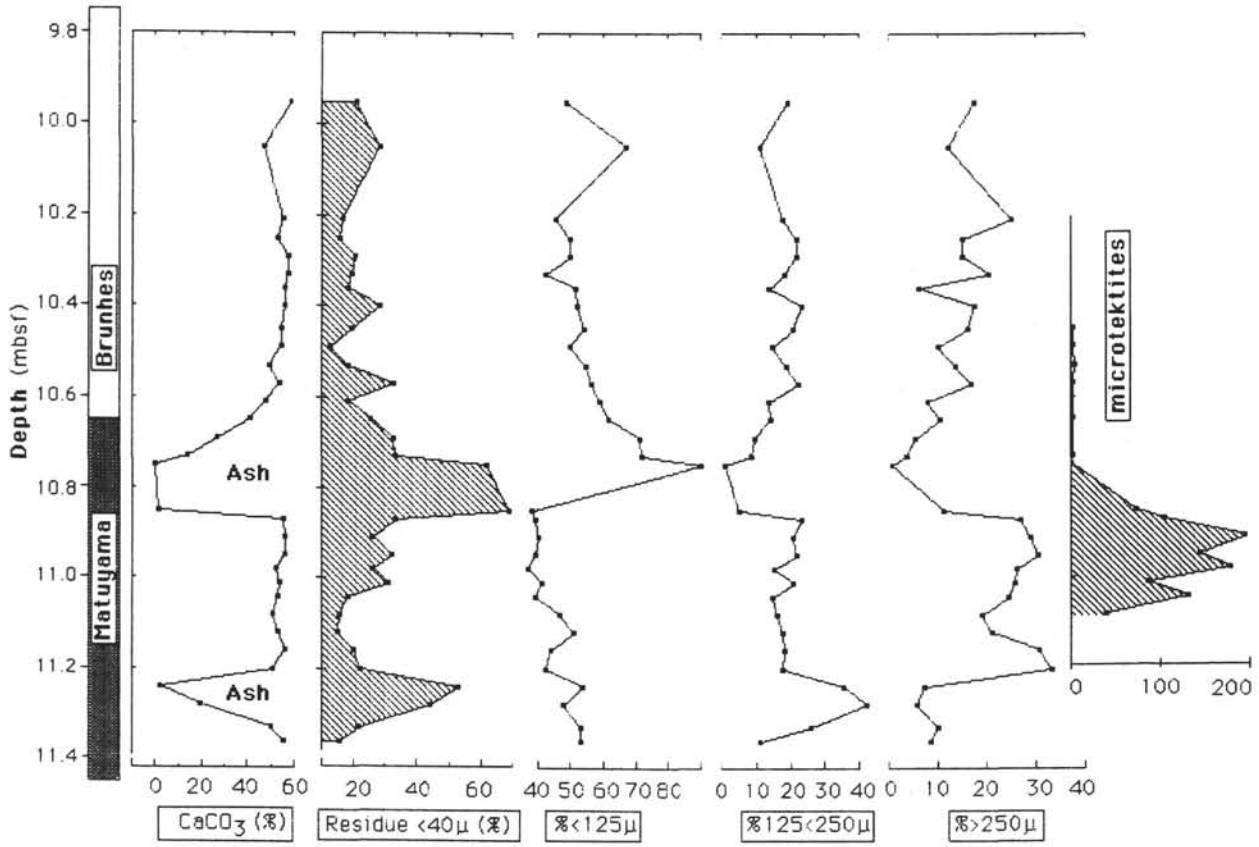

Figure 3. $CaCO_3$ content, weight of washed residue (in wt%) and weight of three different size fractions of the washed residues in percentage of total residue of Sections 121-758B-2H-1 and 121-758B-2H-2. The relative amount of residue >250 mm is considerably larger below and within the microtektite peak.

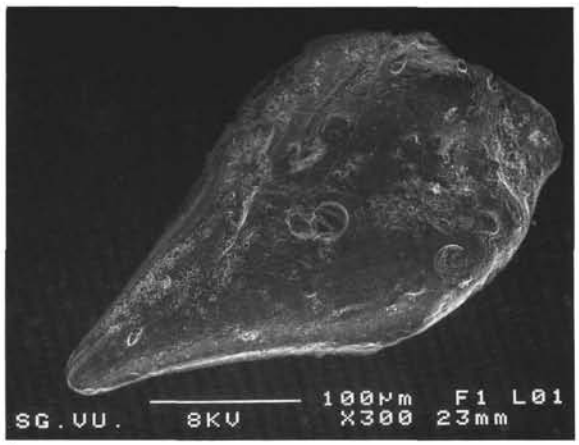

A

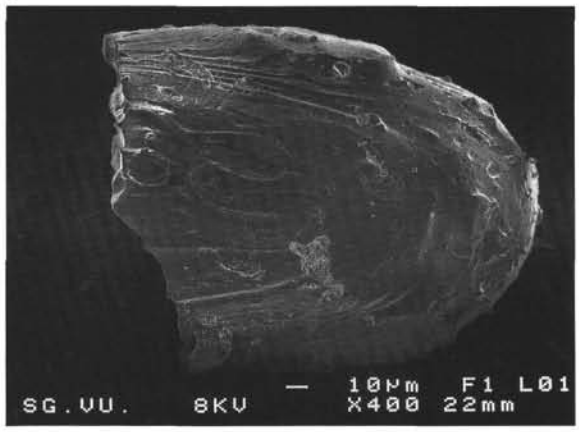

B

C

Figure 4. SEM photomicrographs of microtektite droplets from Sample 121-758B-1H-1, 141–143 cm. All three show flowlines on the surface of the microtektites.

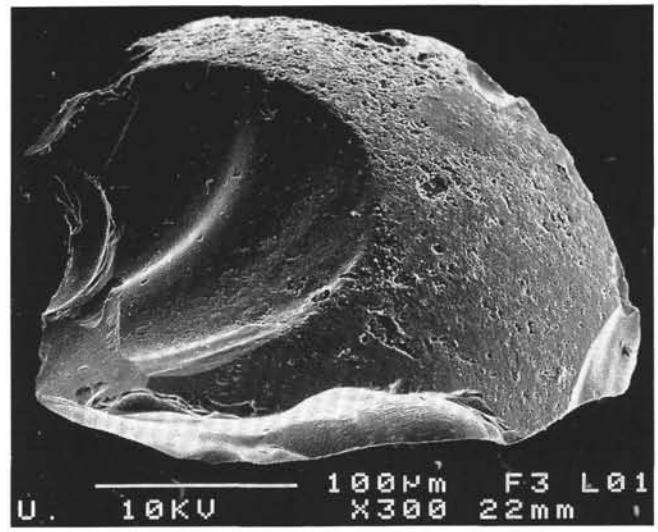

Figure 5. SEM photomicrograph of large, broken microtektite. Sample 121-758B-1H-1, 137–138 cm.

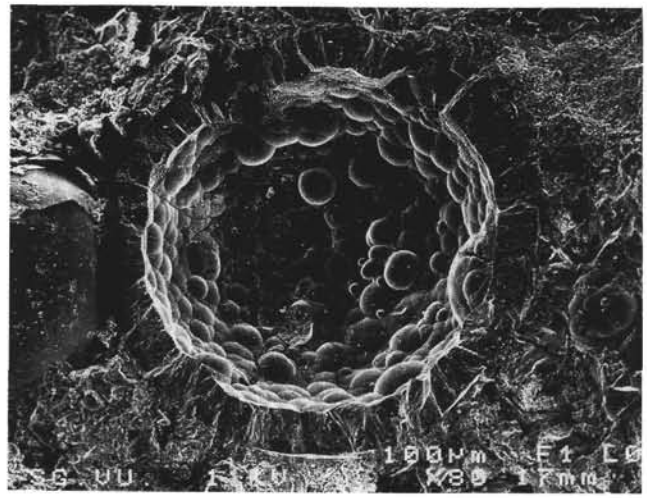

A

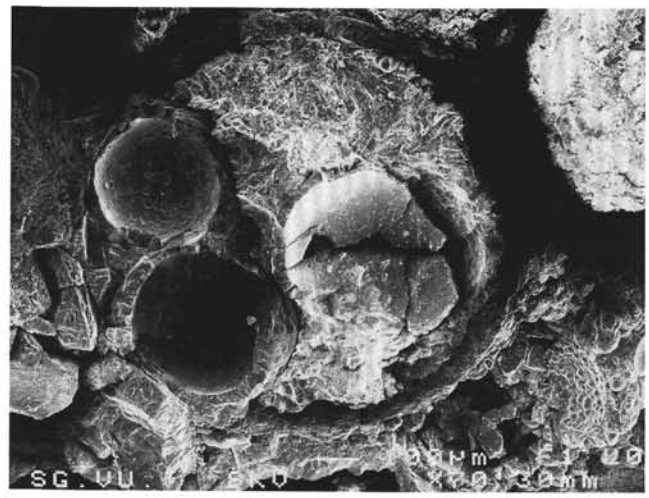

B

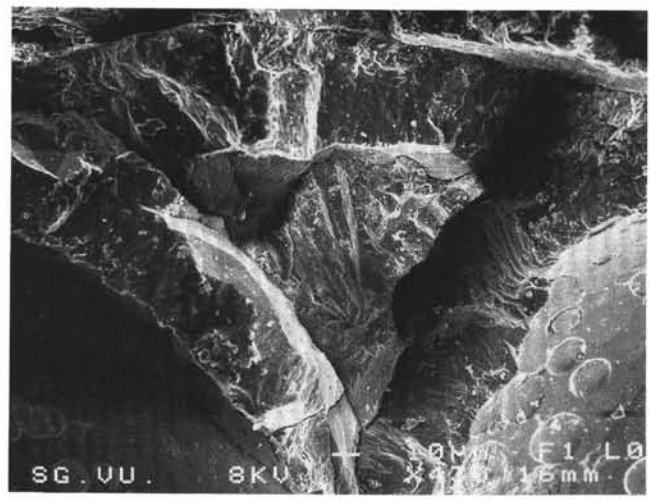

C

Figure 6. SEM photomicrographs of goyazite spherules from the K/Pg boundary of the Dogie Creek locality (Bohor et al., 1987). **A.** Hollow goyazite spherule with mammillary growth of goyazite spherulites toward the interior of the spherule. **B.** Goyazite spherule, with three spherical cavities with smooth interior walls within the spherule. **C.** Enlargement of Figure 6B, showing the goyazite spherulites growing into the interior of the spherule (at the top) and the outward growth of goyazite spherulites from the spherical cavities.

Table 6. INAA data across the K/Pg boundary in Hole 758B.

Depth (mbsf)	Na (%)	K (%)	Ca (%)	Sc	Cr	Fe (%)	Co	Ni	As	Br	Rb	Sr	Sb
356.7	1.7	1.5	7.0	24.1	64.7	5.1	21.8	45.0		16.3	28	1000	0.32
356.9	1.8	1.3		24.9	65.0	7.4	29.6			17.0	35	870	
357.5	1.7	1.6	6.5	27.4	49.9	6.3	27.8		1.7	15.5	42	950	0.90
357.6	1.6	1.2	11.3	23.4	32.4	6.1	24.5	50.0		15.8	27	830	0.60
357.6	1.4	1.5	12.3	18.8	29.1	3.9	16.8		0.9	13.1	31	910	0.50
357.9	1.0	1.0	11.5	12.6	42.2	2.1	11.1	50.0	1.0	8.4	12	710	0.59
358.2	0.5		27.7	2.4	4.4	0.6	2.3			8.9		510	0.19
358.3	0.6	0.7	27.0	9.1	19.5	1.7	5.8	31.0		7.3	12	750	
358.5	1.2	0.8	15.3	16.0	40.6	4.4	17.1		0.9	12.5	16	710	
358.5	0.4	0.2	27.7	5.3	15.6	0.7	14.6		2.0	3.6		490	0.46
358.7	0.2		36.9	1.6	5.1	0.3	2.9	11.0	0.5	5.0		430	0.16
358.8	0.5	0.5	29.8	6.0	23.2	1.1	18.3	48.0	3.6	6.8	10	910	0.47
359.1	0.4	0.3	30.2	2.8	5.7	0.4	2.1			10.1	7	860	
a	1-2	5-10	1-6	1-2	2-9	1-3	1-2	13-26	8-33	1-7	7-15	1-6	7-29

Note: Concentration in μg/g, unless otherwise indicated; a = coefficient of variation of the analytical error (range).

Table 6 (continued).

Cs	Ba (%)	La	Ce	Sm	Eu	Tb	Yb	Lu	Hf	Ta	Th	U	La/Yb
0.43	0.43	9.4	19.8	3.39	0.95	0.57	2.05	0.300	1.83	0.41	1.22		4.6
0.80	0.37	11.2	20.9	3.90	1.12	0.67	2.55	0.400	2.10	0.52	1.29		4.4
0.49	0.28	19.8	39.4	5.80	1.45	0.91	3.14	0.520	3.60	0.78	2.66	1.3	6.3
0.60	0.22	25.2	45.5	6.70	1.57	1.12	3.63	0.580	3.42	1.00	2.77		6.9
0.52	0.22	21.2	35.9	5.20	1.20	0.76	2.73	0.410	3.20	1.00	3.08		7.8
0.53	0.20	15.8	24.0	3.34	0.79	0.57	1.95	0.292	1.54	0.27	0.94		8.1
	0.13	14.0	20.9	2.08	0.35	0.30	1.15	0.193	2.28	0.88	2.82		12.2
	0.28	14.1	21.2	2.85	0.67	0.47	2.00	0.317	0.86	0.32	0.59		7.1
0.32	0.21	12.9	16.4	2.82	0.80	0.46	1.90	0.242	1.47	0.30	0.76	1.5	6.8
	0.13	15.0	15.9	2.34	0.57	0.38	1.31	0.207	0.38		0.30	1.7	11.5
0.07	0.03	6.8	6.9	0.91	0.21	0.16	0.67	0.103	0.27	0.09	0.26		10.1
0.33	0.10	14.0	12.9	2.68	0.66	0.46	1.60	0.269	1.10	0.28	1.19		8.8
0.23	0.11	11.9	7.9	2.06	0.48	0.31	1.19	0.190	0.52	0.10	0.44		10.0
7-29	1-7	1-2	2-4	1-2	1-4	3-7	1-3	2-5	3-30	3-23	2-5	10-28	

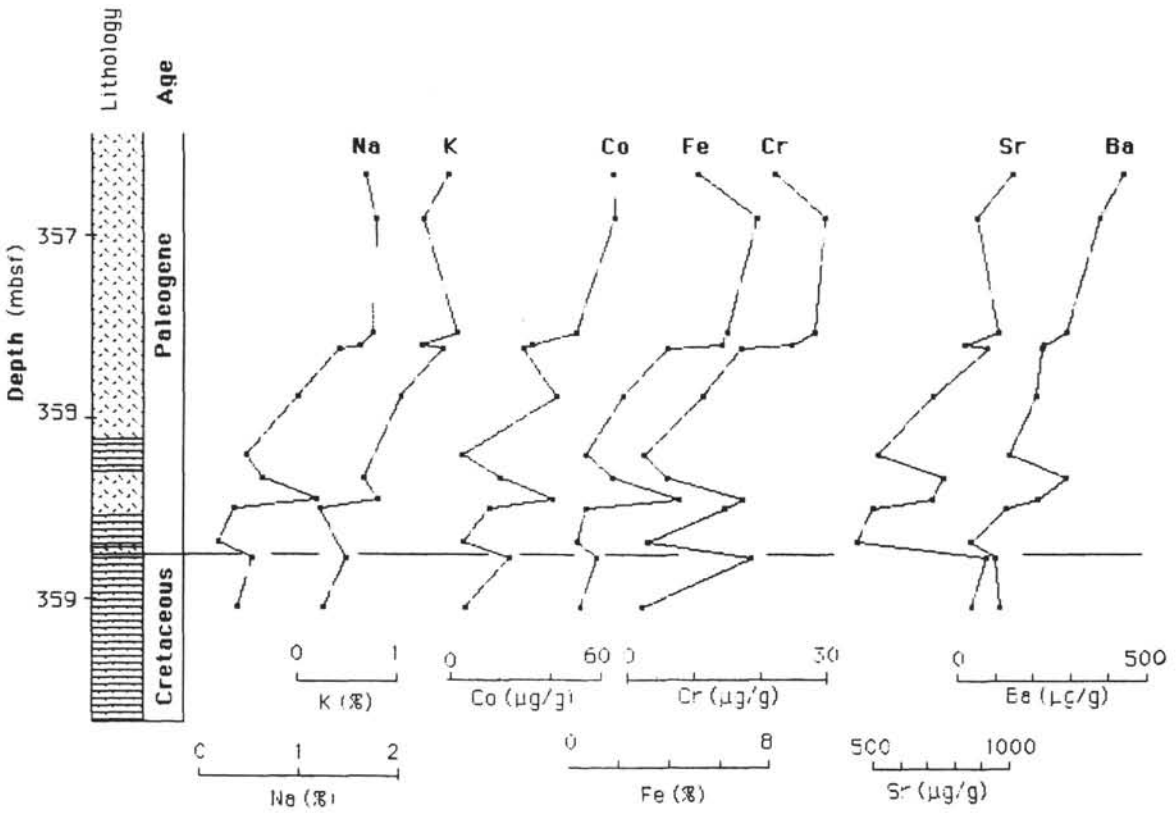

Figure 7. Concentrations of Na, K, Co, Fe, Cr, Sr, and Ba determined by instrumental neutron activation analysis (INAA) across the K/Pg boundary in Sections 121-752B-11R-2 and 121-752B-11R-3. These elements show a trend that is similar to the measured volume magnetic susceptibility, and are thus closely related with volcanic ash content.

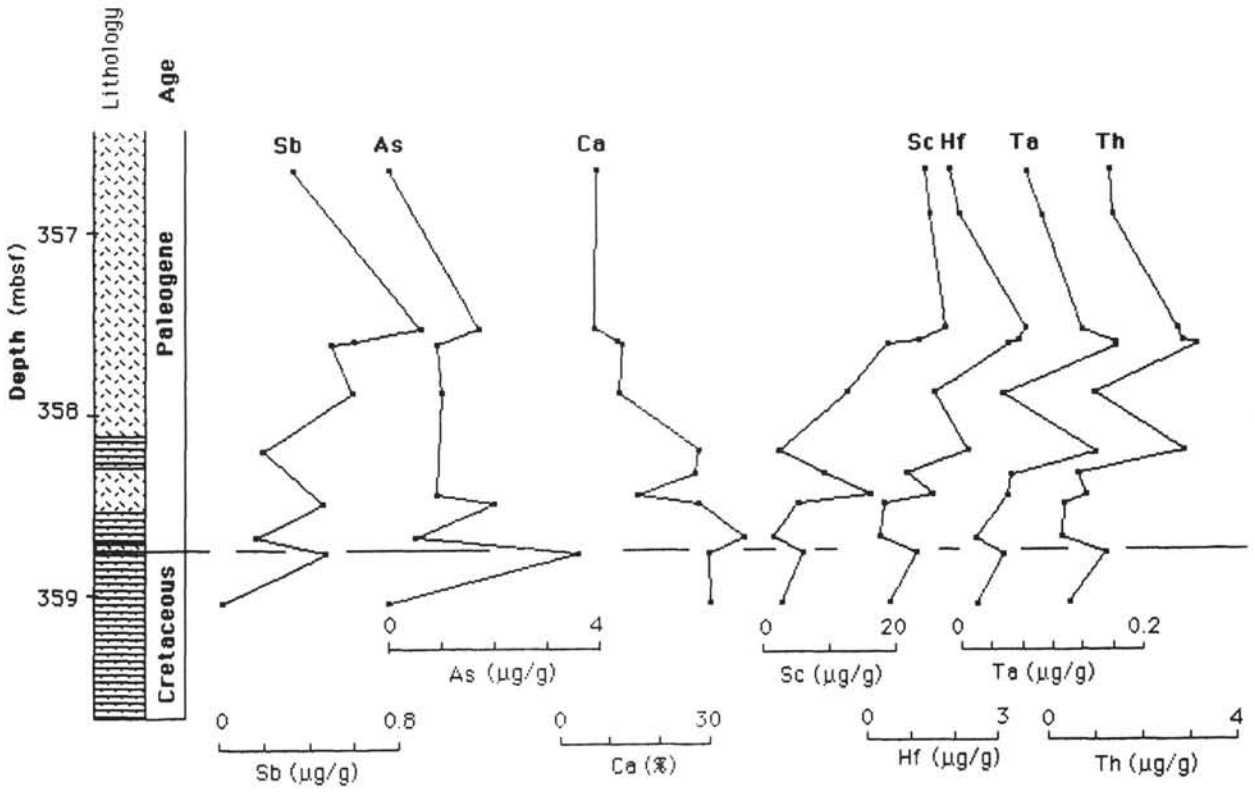

Figure 8. Concentrations of Sb, As, Ca, Sc, Hf, Ta, and Th determined by INAA across the K/Pg boundary in Sections 121-752B-11R-2 and 121-752B-11R-3. Only As shows a peak at the K/Pg boundary, but it is not anomalously high. Sc, Hf, Ta, and Th generally increase with increasing volcanic ash content.

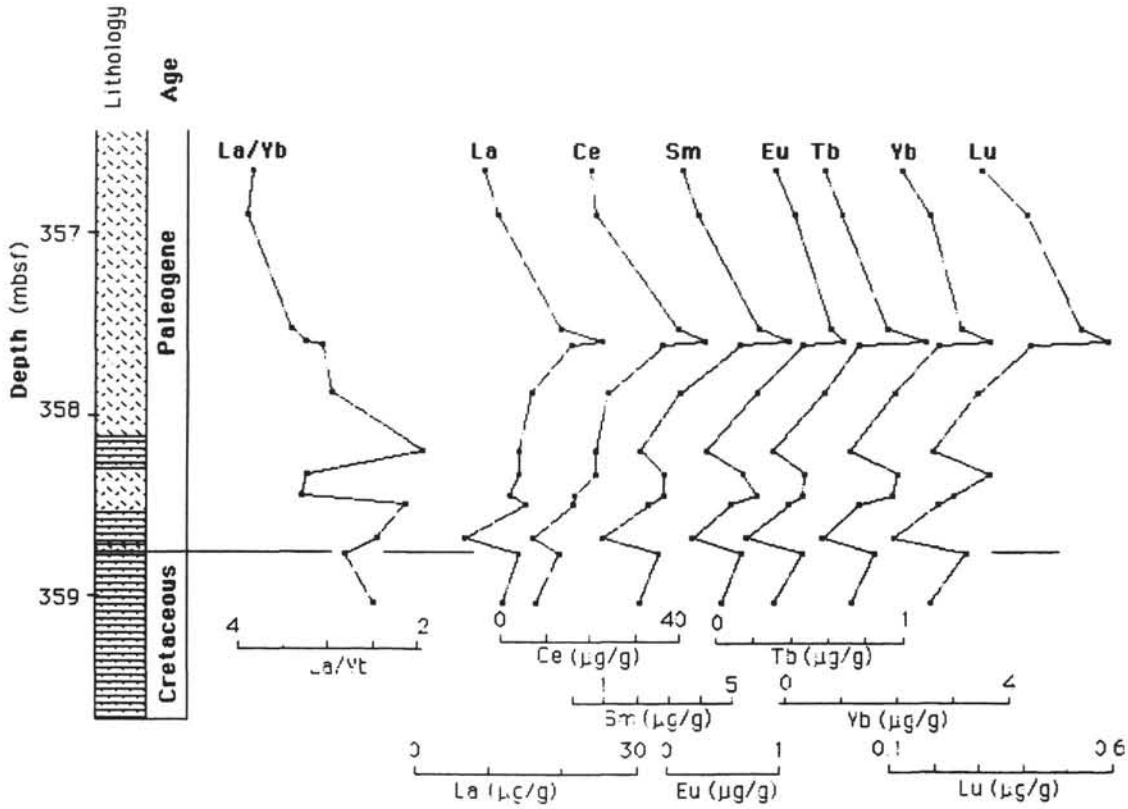

Figure 9. Concentrations of REE determined by INAA across the K/Pg boundary in Sections 121-752B-11R-2 and 121-752B-11R-3. The REE abundances have no obvious relation to the K/Pg boundary, or to volcanic ash content. The heavy REE are clearly more abundant in the ash-rich samples, which leads to a consistently low La/Yb in the ash and high La/Yb in the chalks.

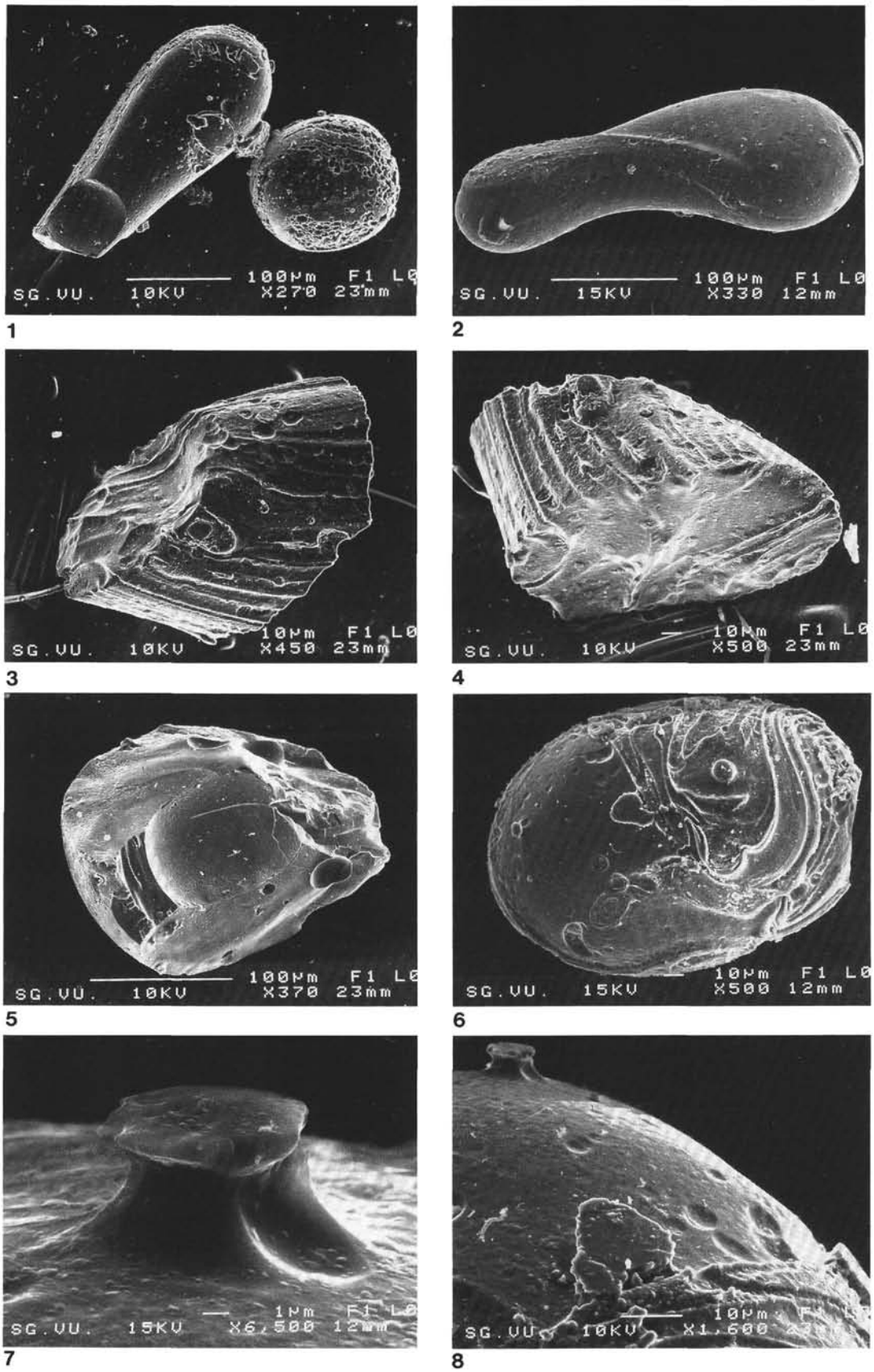

Plate 1. SEM photomicrographs of microtektites from Sample 121-758B-2H-1, 141–143 cm. **1.** Droplet and sphere. **2.** One of the rare dumbbells. **3, 4.** Broken droplet with flowlines on the surface, which continue over fracture face. **5.** Broken sphere, with many bubble cavities in the interior (see also text Fig. 6). **6.** Spheroid with etched-out flowlines. **7, 8.** Enlargements of (6), showing the etching of the surface, which resulted in relict, isolated "buttes" on the surface.

1

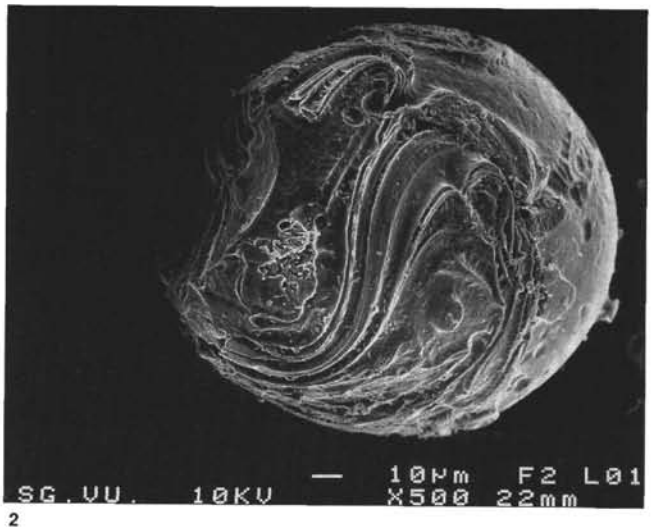

2

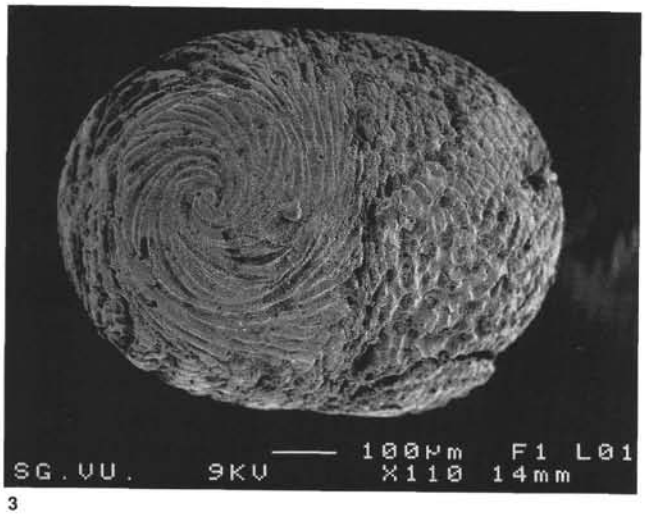

3

4

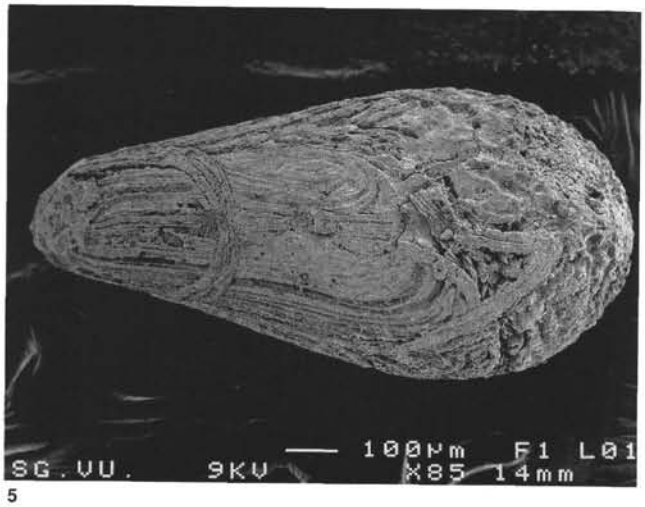

5

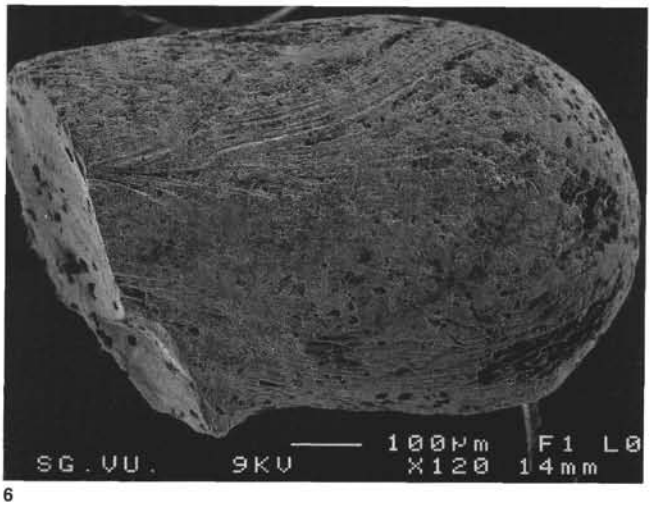

6

Plate 2. SEM photomicrographs of Australasian microtektites from Sample 121-758B-2H-1, 141–143 cm, and goyazite spherules from the K/Pg boundary of Dogie Creek, Wyoming, (Bohor et al., 1987). **1, 2.** Spheroids from Hole 758B, with flowlines on the surface. **3, 4.** Goyazite spheroid from Dogie Creek with preserved flowlines. **5, 6.** Goyazite droplets from Dogie Creek with flowlines.